

Improved dendroclimatic calibration using blue intensity in the southern Yukon

The Holocene
1–14

© The Author(s) 2019


Article reuse guidelines:

sagepub.com/journals-permissions

DOI: 10.1177/0959683619862037

journals.sagepub.com/home/hol



**R Wilson,^{1,2}  K Anchukaitis,^{2,3,4} L Andreu-Hayles,² E Cook,²
R D'Arrigo,² N Davi,^{2,5} L Haberbauer,¹ P Krusic,^{6,7} B Luckman,⁸
D Morimoto,⁹ R Oelkers,² G Wiles¹⁰ and C Wood¹**

Abstract

In north-western North America, the so-called divergence problem (DP) is expressed in tree ring width (RW) as an unstable temperature signal in recent decades. Maximum latewood density (MXD), from the same region, shows minimal evidence of DP. While MXD is a superior proxy for summer temperatures, there are very few long MXD records from North America. Latewood blue intensity (LWB) measures similar wood properties as MXD, expresses a similar climate response, is much cheaper to generate and thereby could provide the means to profoundly expand the extant network of temperature sensitive tree-ring (TR) chronologies in North America. In this study, LWB is measured from 17 white spruce sites (*Picea glauca*) in south-western Yukon to test whether LWB is immune to the temporal calibration instabilities observed in RW. A number of detrending methodologies are examined. The strongest calibration results for both RW and LWB are consistently returned using age-dependent spline (ADS) detrending within the signal-free (SF) framework. RW data calibrate best with June–July maximum temperatures (Tmax), explaining up to 28% variance, but all models fail validation and residual analysis. In comparison, LWB calibrates strongly (explaining 43–51% of May–August Tmax) and validates well. The reconstruction extends to 1337 CE, but uncertainties increase substantially before the early 17th century because of low replication. RW-, MXD- and LWB-based summer temperature reconstructions from the Gulf of Alaska, the Wrangell Mountains and Northern Alaska display good agreement at multi-decadal and higher frequencies, but the Yukon LWB reconstruction appears potentially limited in its expression of centennial-scale variation. While LWB improves dendroclimatic calibration, future work must focus on suitably preserved sub-fossil material to increase replication prior to 1650 CE.

Keywords

age-dependent spline, blue intensity, summer temperature reconstruction, tree ring, white spruce, Yukon

Received 18 January 2019; revised manuscript accepted 5 June 2019

Introduction

In recent years, substantial gains have been made by the dendroclimatic community to reconstruct past summer temperatures over the Northern Hemisphere (NH) (Anchukaitis et al., 2017; Guillet et al., 2017; Schneider et al., 2015; Stoffel et al., 2015; Wilson et al., 2016). These reconstructions not only enhance our knowledge of the transition from the Medieval to the Little Ice Age periods, but have proven crucial in providing refined estimates of post-volcanic cooling at hemispheric scales. The spatial representation of past NH summer temperatures (Anchukaitis et al., 2017; Guillet et al., 2017) clearly shows large regions that are not well reconstructed simply because of a lack of data. North America is particularly poorly constrained with only three tree-ring (TR) records extending prior to 1000 CE (Canadian Rockies – Luckman and Wilson, 2005; Quebec – Gennaretti et al., 2014 and the Gulf of Alaska – Wiles et al., 2014). The latter two use tree-ring width (TRW) data, while only Luckman and Wilson (2005) utilise maximum latewood density (MXD), a metric shown to be more robust than RW for reconstructing past summer temperatures (Anchukaitis et al., 2012, 2013; Briffa et al., 2002; Büntgen et al., 2006; Esper et al., 2012; Luckman and Wilson, 2005; Schweingruber and Briffa, 1996; Wilson et al., 2016; Wilson and Luckman, 2003).

Despite the efficacy of wood density parameters to reconstruct past summer temperature, there is a surprising paucity of long MXD records around the mid-to-high latitudes of the NH (Anchukaitis et al., 2017; Wilson et al., 2016). Unfortunately, few

institutions worldwide have the facilities to measure density from dendrochronological samples. A relatively new TR parameter, latewood blue intensity (LWB), may provide complementary information to MXD at a fraction of the cost, making LWB an

¹School of Earth and Environmental Sciences, University of St Andrews, Scotland, UK

²Lamont-Doherty Earth Observatory of Columbia University, NY, USA

³School of Geography and Development, The University of Arizona, Tucson, AZ, USA

⁴Laboratory of Tree-Ring Research, The University of Arizona, Tucson, AZ, USA

⁵Department of Environmental Science, William Paterson University, Wayne, NJ, USA

⁶Department of Geography, University of Cambridge, Cambridge, UK

⁷Department of Physical Geography, Stockholm University, Stockholm, Sweden

⁸Department of Geography, The University of Western Ontario, London, ON, Canada

⁹Department of Geography and Tourism Studies, Brock University, St. Catharines, ON, Canada

¹⁰Department of Earth Sciences, The College of Wooster, Wooster, OH, USA

Corresponding author:

R Wilson, School of Earth and Environmental Sciences, University of St Andrews, North Street, St Andrews, Scotland KY16 9AL, UK.

Email: rjsw@st-andrews.ac.uk

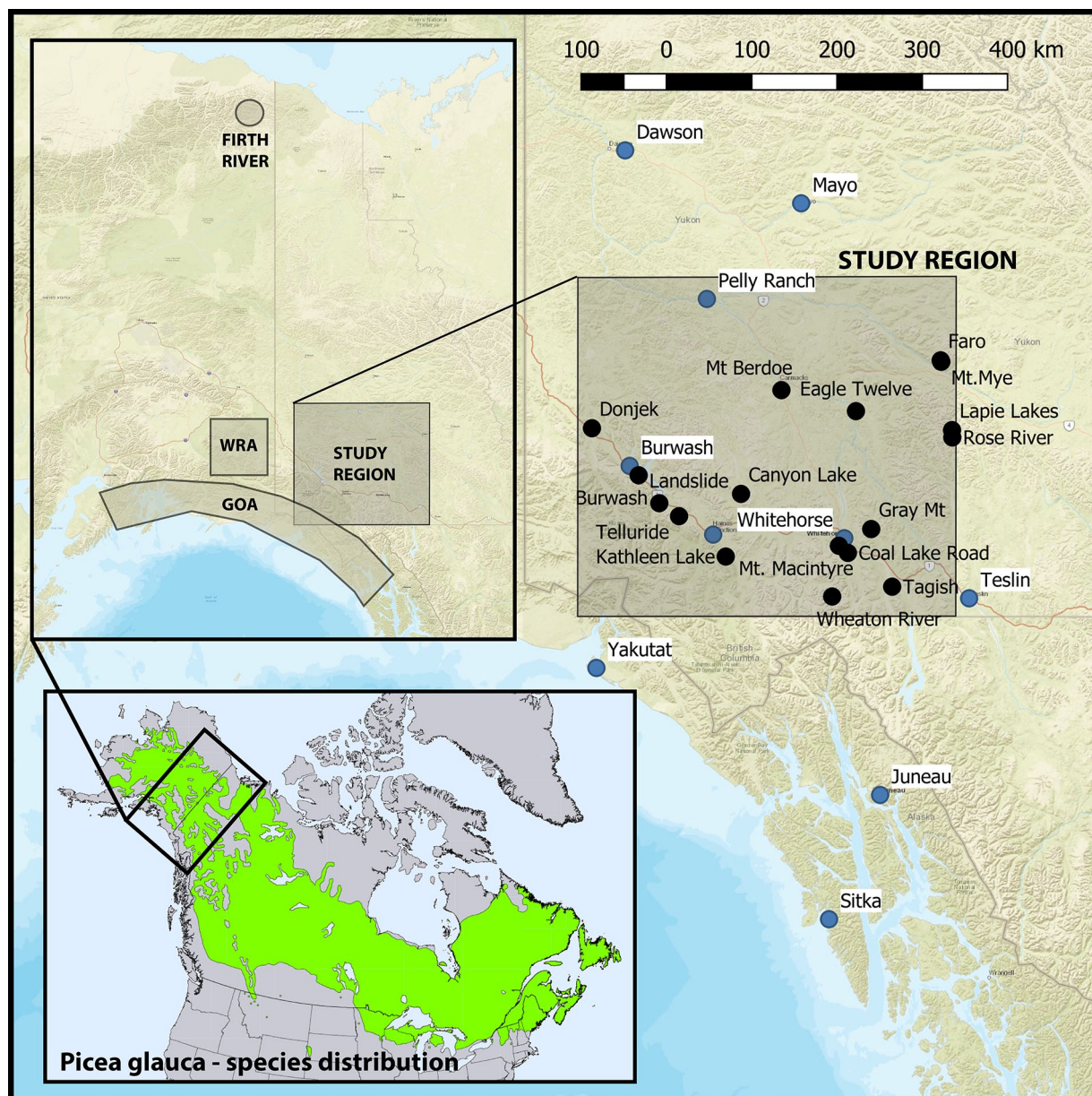


Figure 1. Location map showing the 17 tree-ring sites (black) and instrumental stations (blue). The 'Study Region' box denotes the CRU TS 4.01 gridded (60–63 N/140–133 W) temperature data (Harris et al. 2014) used for dendroclimatic analyses. Also shown is the spatial distribution of *Picea glauca* (white spruce) and the locations of the regional reconstructions compared in Figure 9.

affordable compromise for any Tree-Ring laboratory (see Björklund et al. (2014, 2015), Buckley et al. (2018), Campbell et al. (2007), McCarroll et al. (2002) and Rydval et al. (2014) for a detailed description of LWB and related parameters). LWB expresses similar information to MXD as both essentially measure the combined hemicellulose, cellulose and lignin content of the latewood, which is well correlated with summer temperatures. LWB (and related reflectance parameter) chronologies have been successfully used in several summer temperature reconstructions (Björklund et al., 2015; Fuentes et al., 2018; Rydval et al., 2017a, 2017b; Wilson et al., 2014, 2017). However, LWB is arguably still an experimental TR parameter and more studies are needed to evaluate its utility for different tree species and across multiple regions. One obvious limitation is that any colour variation that is not representative of climatic processes affecting cell wall thickness will bias LWB measurements. For example, compared with its living sample counterpart, remnant snag or sub-fossil wood is often darker, leading to lower reflectance intensity values, and a warm bias in calibrated temperature estimates. Similarly, many conifer species express a distinct colour change between darker

heartwood to lighter sapwood, again inducing low-frequency related colour intensity biases. Multiple methods have been proposed to overcome these potential biases, but application of these approaches remains limited (Björklund et al., 2014, 2015; Rydval et al., 2017a, 2017b; Wilson et al., 2017).

This study focuses on exploring the dendroclimatic utility of LWB from white spruce (*Picea glauca*), that grows across much of the North American boreal forest (Figure 1). White spruce manifests no demonstrable colour change between its heartwood and sapwood, making it a good candidate species for LWB-based dendroclimatology (Björklund et al., 2014, 2015; Wilson et al., 2017). Here, we detail the development of a new extended, southern Yukon, summer temperature reconstruction. This record builds on previous research by Youngblut and Luckman (2008) who developed an RW-based June–July maximum temperature (T_{max}) reconstruction (1684–1995) from seven spruce sites. Our aim is to assess whether LWB is a more robust parameter for reconstructing past summer temperatures than RW. Previous work has shown that the temperature signal in many RW datasets throughout north-western North America is not temporally stable (Andreu-Hayles et al.,

Table 1. Site information: location, elevation and number of series measured per site/variable.

| Site name | Latitude | Longitude | Elevation (m a.s.l.) | RW no. of series | RW time-span | LWB no. of series | LWB time-span |
|-----------------------------|------------|-------------|-------------------------|---------------------|--------------|----------------------|------------------|
| Mt Mye | 62°16'44"N | 133°15'59"W | 1205 | 64 | 1573–2005 | 23 | 1578–2004 |
| Faro | 62°17'30"N | 133°16'40"W | 1205 | 105 | 1229–2004 | 40 | 1229–2003 |
| Lapie Lakes | 61°40'60"N | 133°4'0"W | 1083 | 41 | 1639–2005 | 41 | 1639–2004 |
| Rose River | 61°37'8"N | 133°3'44"W | 1085 | 27 | 1595–2005 | 27 | 1595–2004 |
| Eagle 12* | 61°51'0"N | 134°50'60"W | 1130 | 78 | 1607–1999 | 28 | 1606–1998 |
| Tagish | 60°16'25"N | 134°10'41"W | 1167 | 34 | 1567–2005 | 34 | 1567–2004 |
| Telluride* | 60°54'60"N | 138°7'60"W | 1400 | 89 | 1584–1998 | 30 | 1659–1997 |
| Landslide | 61°1'60"N | 138°30'0"W | 800 | 189 | 913–2001 | 148 | 914–2000 |
| Burwash* | 61°16'60"N | 138°52'60"W | 840 | 79 | 1480–1999 | 29 | 1570–1998 |
| Canyon Lake* | 61°7'0"N | 136°59'0"W | 900 | 43 | 1651–1998 | 22 | 1692–1997 |
| Mt Berdoe | 62°1'60"N | 136°13'60"W | 1170 | 35 | 1618–2001 | 34 | 1676–2000 |
| Wheaton River | 60°10'60"N | 135°17'30"W | 1032 | 60 | 1666–2004 | 54 | 1665–2003 |
| Grey Mountain (Whitehorse)* | 60°48'0"N | 134°34'0"W | 1140 | 92 | 1512–1999 | 33 | 1746–1998 |
| Mt. McIntyre | 60°38'52"N | 135°10'1"W | 1232 | 51 | 1618–2003 | 20 | 1651–2002 |
| Coal Lake Road | 60°35'0"N | 135°0'0"W | 1070 | 47 | 1729–2003 | 32 | 1729–2002 |
| Kathleen Lake | 60°32'60"N | 137°16'0"W | 750 | 62 | 1625–1998 | 23 | 1667–1997 |
| Donjek | 61°41'60"N | 139°45'0"W | 750 | 56 | 1614–1998 | 17 | 1746–1997 |

RW: ring width; LWB: latewood blue intensity.

*Site used in Youngblut and Luckman (2008).

2011; Davi et al., 2003; Jacoby and D'Arrigo, 1995; Porter and Pisaric, 2011; Wilson and Luckman, 2003). This phenomenon is one aspect of the multifaceted issue often referred to as the 'Divergence Problem' (DP; D'Arrigo et al., 2008). Studies using MXD chronologies from northern Yukon/Alaska and Alberta/British Columbia suggest that this variable is less prone to DP (Anchukaitis et al., 2013; Andreu-Hayles et al., 2011; Luckman and Wilson, 2005; Wilson et al., 2014; Wilson and Luckman, 2003). Therefore, as LWB behaves similarly to MXD, we hypothesise that LWB is likely a superior parameter to RW for reconstructing past summer temperatures in the southern Yukon.

Materials and methods

RW and LWB data were measured from a network of 17 white spruce sites (Figure 1 and Table 1) in south-western Yukon sampled during multiple field campaigns between 1999 and 2006. The sites were sampled along a range of elevations from 750 to 1400 m a.s.l. with generally gentle slopes of 5–15°. The sites showed no evidence of spruce bark beetle infestation and, where possible, site ecological characteristics were kept consistent (similar shrub understory and soil types) across the network except for a few notable locations (see later discussion). The study region is roughly a 400 × 300 km area, ensuring substantial future potential for chronology extension using remnant sub-fossil material extracted from lakes in the area. As spruce shows no obvious colour change across the heartwood/sapwood boundary, no resin extraction was performed. Samples were sanded to 1200 grit and scanned to 3200 dpi on an Epson V850 scanner calibrated using an IT8.7/2 colour card in conjunction with the SilverFast scanning software. Rings were measured and cross-dated using the CooRecorder/CDendro 8.1 software and RW and LWB generated (Cybis 2016, <http://www.cybis.se/forfun/dendro/index.htm> – see Rydval et al. (2014) and Buckley et al. (2018) for more details on LWB generation using CooRecorder). As is the 'undocumented' norm for density measurements, the last complete ring of each sample was not measured because of its darker nature – a consequence of proximity to the cambium. The raw LWB measurements were inverted to allow detrending of the data by methods similar to those used for MXD data (Rydval et al. 2014). To minimise the effects of discolouration and reaction wood, LWB was often measured on a subset of samples that showed no reaction wood or areas of discolouration (see Table 1).

Standardisation is a crucial data processing step in dendroclimatology, which aims to remove non-climatic age-related trends while retaining the desired climatic signal (Cook et al., 1990). However, we do not believe that the dendroclimatic community fully appreciates the impact of the detrending method 'choice' on both the calibration and validation results (for more discussion, see Esper et al. (2007), Sullivan et al. (2016) and Wilson et al. (2017). Therefore, the RW and LWB data were detrended using a range of methods, from the traditional negative exponential and linear functions (Fritts, 1976) to the relatively novel age-dependent spline (ADS) method (Melvin et al., 2007) (see Table 2 for details). The sensitivity of using the 'signal-free' (SF) method of Melvin and Briffa (2008) was also explored for each detrending option. The SF method is a major advance in the detrending of TR data because it recovers common medium-frequency variability on timescales longer than the series' lengths (decades to a century or longer) that may have been inadvertently removed by the initial data detrending (Cook et al., 1995).

The ADS (Melvin et al., 2007) is another important recent advance in detrending TR series because it more naturally tracks the long-term trajectory of radial growth than the rigidly defined, modified negative exponential curve (NE) (Fritts et al., 1969). When using a NE, there can be a systematic lack of fit as the tree ages, which is largely an artefact of the model's fixed asymptote. This is the reason why Holmes et al. (1986) introduced double-detrending, to minimise this systematic lack of fit that was unlikely because of climate. The ADS is far less likely to introduce such artefacts into the detrended series because of the very natural way it tracks the trajectory of radial growth as the tree ages. However, some adjustment in how the ADS is fitted is still necessary, particularly if there is an *a priori* expectation that tree growth, because of climate (e.g. from a warming climate in the 20th century), should systematically increase over several decades. If left unconstrained, the ADS will track this growth trend because of climate and thus diminish or remove it from the resulting TR chronology. It is for this reason that the ADS is applied here with an option that constrains its end behaviour to be non-increasing. The combination of SF and ADS, with this non-increasing constraint, greatly reduces the potential loss of a climate warming signal in the TRs. This should apply equally to both the RW and LWB data evaluated here for producing a summer temperature reconstruction.

The Expressed Population Statistic (EPS – Wigley et al., 1984) was used to evaluate the quality of the chronologies, as well as estimating the number of series needed to attain a reasonable expression of the theoretical infinitely replicated population chronology (Wilson

Table 2. Detrending methods used for either RW or LWB data or both (RW/LWB).

| Parameter | Code | Description |
|-----------|-----------|-----------------------------------------------------------------------|
| RW | NEPT | Negative exponential or regression slope of neg trend after PT |
| RW | NEPT-sf | NEPT with SF |
| LWB | NEGREG | Negative regression (or zero slope) regression with PT |
| LWB | NEGREG-sf | NEGREG with SF |
| RW / LWB | ADSvar | Age-dependent spline (allow pos and neg trend removal) with PT |
| RW / LWB | ADSvar-sf | Age-dependent spline (allow pos and neg trend removal) with PT and SF |
| RW / LWB | ADSne | Age-dependent spline (allow only neg trend removal) with PT |
| RW/LWB | ADSne-sf | Age-dependent spline (allow only neg trend removal) with PT and SF |

RW: ring width; LWB: latewood blue intensity; PT: power transform; SF: signal-free.

Table 3. Station data (mean temperatures) within or proximal to the CRU TS 4.01 grid (60–63°N/140–133°W) used. See Figure 1 for locations.

| Site name | Latitude | Longitude | Elevation (m a.s.l.) | Start year |
|-----------------|----------|-----------|----------------------|------------|
| Pelly Ranch | 62°49'N | 137°37'W | 454 | 1955 |
| Burwash | 61°22'N | 139°03'W | 807 | 1967 |
| Haines Junction | 60°45'N | 137°30'W | 596 | 1945 |
| Whitehorse | 60°43'N | 135°04'W | 706 | 1943 |
| Teslin | 60°10'N | 132°45'W | 705 | 1944 |
| Mayo | 63°37'N | 135°52'W | 504 | 1925 |
| Dawson | 64°03'N | 139°08'W | 370 | 1898 |
| Yakutat | 59°31'N | 139°4'W | 9 | 1917 |
| Juneau | 58°17'N | 134°24'W | 8 | 1881 |
| Sitka | 57°04'N | 135°21'W | 20 | 1828 |

and Elling, 2004). The spatial homogeneity of the between-chronology signal was assessed using principal component analysis (PCA) over the well-replicated common period (1856–1997) and by examining the spatial loadings of the individual chronologies on the leading mode of covariability (i.e. the first principal component).

For climate analyses, we used gridded CRU TS 4.01 (Harris et al., 2014) mean (Tmean) and maximum (Tmax) temperature data over the area 60–63°N/140–133°W, which represents the region where the TR sites are located (Figure 1). The results using minimum temperatures are not shown as correlations with the TR variables are substantially weaker. It is important to note that of the five individual meteorological stations within this region, the earliest measurements were made in 1943 (i.e. Whitehorse; Table 3). Consequently, all Tmean and Tmax data prior to the 1940s are interpolations from stations located farther away, including Dawson to the north, and three stations from the Gulf of Alaska to the south (Yakutat, Juneau and Sitka – see Figure 1), which may arguably represent subtly different regional climates.

The climate response of the RW and LWB chronologies was assessed by correlating individual and regional composite chronologies with Tmean and Tmax. Analyses were performed over the years 1944–1997, the period represented by at least two stations (Table 3) and the outer date of the earliest sampled site chronologies. The 1944–1997 period was also used for reconstruction calibration, while validation was performed on the combined 1901–1943/1998–2004 period. Reconstruction validations were assessed by the performance of the Pearson's correlation coefficient (r), the reduction of error (RE), and the coefficient of efficiency (CE; Cook et al., 1994). Residual analyses, exploring for linear trends and first-order autocorrelation (Durbin-Watson statistic), were also performed over the 1944–1997 period.

Results and discussion

Signal strength and homogeneity

RW has a stronger common signal than LWB as measured by the mean interseries correlation (RBAR) and the expressed population

signal (EPS – Table 4) – an observation noted in other studies (Rydval et al., 2014; Wilson et al., 2017, 2017). The median RBAR for RW, using the 17 sites, is 0.30 (range 0.21–0.47), and for LWB it is 0.18 (range 0.10–0.23). The median number of trees needed to attain an EPS value of 0.85 (Wigley et al., 1984; Wilson and Elling, 2004) is 13 and 26 for RW and LWB, respectively. This seemingly weaker between-tree common signal and larger sample size requirement for LWB is not deemed to be a problem, at least for recent centuries, as all the data from the whole region are combined to create a well-replicated regional composite for generating the final dendroclimatic reconstruction. However, for studies which might utilise individual sites, these signal strength metrics indicate that, on average, a minimum of 25–30 trees per site is needed to ensure good signal fidelity in the LWB chronologies. However, it should be noted that several studies have found that despite having a weak common signal, the resulting LWB chronologies still possess a consistently stronger climate signal than RW (Rydval et al., 2014; Wilson et al., 2014, 2017).

Since many of the LWB chronologies are not replicated enough to attain a site-level EPS > 0.85 (see Tables 1 and 4), PCA was performed separately for RW and LWB over the 1856–1997 period, when replication is at least 15 trees. The spatial pattern of site chronology loading on the first principal component (PC1) is very similar for both variables (Figure 2). The explained variance on the first eigenvector is 58.4% and 51.9% for RW and LWB, respectively. For both TR parameters, there is a tendency for the lower elevation sites to load weakly on PC1 (Figure 2). Although this might represent a change in climate response from high elevation temperature sensitive tree-line sites to drier lower elevations (see later discussion), some caution is advised with this interpretation as some of the lower elevation sites are rather ecologically unique compared with the wider network. For example, Donjek is located on a gravel terrace, while Landslide is predominantly an arid rocky site with thin soils.

To maximise EPS, the individual site data were pooled to create regional composite records for both TR variables. This approach was used by Youngblut and Luckman (2008). Such a well-replicated dataset leads to a robust final chronology in which the sensitivity to different detrending options can be evaluated. The RW regional composite variants (Figure 3) show strong overall signal strength (EPS > 0.85) back to 1200 CE, but substantial variation arises from using different detrending methods. The ADSvar (Table 2) versions, which allow for removal of both the negative and positive trends, express much less long-term secular amplitude changes compared with the NEPT-sf version, which shows substantially lower index values around the 17th and 18th centuries. EPS values for the LWB regional composite chronology drop below 0.85 in the 17th century, but hover around 0.7 until the 14th century where there is a marked weakening in the EPS prior to the mid-1300s. Compared with the RW data, there is much less variation between the final LWB chronology variants, and there appears to be less long-term centennial trends. Hereafter, we use the regional composite chronologies from 1337 CE after which the LWB data are replicated by at least 15 trees.

Table 4. RBAR and the number of series needed to attain an EPS of 0.85. For RBAR values, RW and LWB data were detrended using the ADSne-sf version. Also shown is the first year for each site when sample replication is ≥ 15 series.

| Site name | RW RBAR | No. series EPS 0.85 | RW year, $n \geq 15$ | LWB RBAR | No. of series EPS 0.85 | LWB year, $n \geq 15$ |
|-----------------------------|-------------|---------------------|----------------------|-------------|------------------------|-----------------------|
| Mt Mye | 0.26 | 16.4 | 1678 | 0.14 | 35.2 | 1809 |
| Faro | 0.28 | 14.9 | 1510 | 0.11 | 45.4 | 1704 |
| Lapie Lakes | 0.21 | 20.8 | 1788 | 0.10 | 49.1 | 1788 |
| Rose River | 0.34 | 11.2 | 1848 | 0.17 | 26.8 | 1848 |
| Eagle 12 | 0.26 | 16.4 | 1769 | 0.18 | 25.0 | 1769 |
| Tagish | 0.37 | 9.5 | 1801 | 0.22 | 20.2 | 1801 |
| Telluride | 0.31 | 12.8 | 1769 | 0.21 | 21.3 | 1769 |
| Landslide | 0.39 | 8.9 | 1158 | 0.19 | 23.8 | 1356 |
| Burwash | 0.30 | 13.1 | 1724 | 0.18 | 25.8 | 1724 |
| Canyon Lake | 0.29 | 14.0 | 1772 | 0.19 | 23.5 | 1772 |
| Mt Berdoe | 0.31 | 12.7 | 1800 | 0.13 | 39.1 | 1800 |
| Wheaton River | 0.46 | 6.6 | 1756 | 0.21 | 21.8 | 1756 |
| Gray Mountain (White Horse) | 0.28 | 14.5 | 1801 | 0.18 | 25.7 | 1801 |
| Mt. McIntyre | 0.22 | 19.5 | 1778 | 0.23 | 18.8 | 1856 |
| Coal Lake Road | 0.42 | 8.0 | 1776 | 0.13 | 37.4 | 1776 |
| Kathleen Lake | 0.29 | 14.0 | 1779 | 0.17 | 28.6 | 1799 |
| Donjek | 0.47 | 6.3 | 1849 | 0.14 | 33.8 | 1849 |
| Median | 0.30 | 13.1 | | 0.18 | 25.81 | |

RW: ring width; RBAR: mean interseries correlation; EPS: Expressed Population Statistic; LWB: latewood blue intensity.

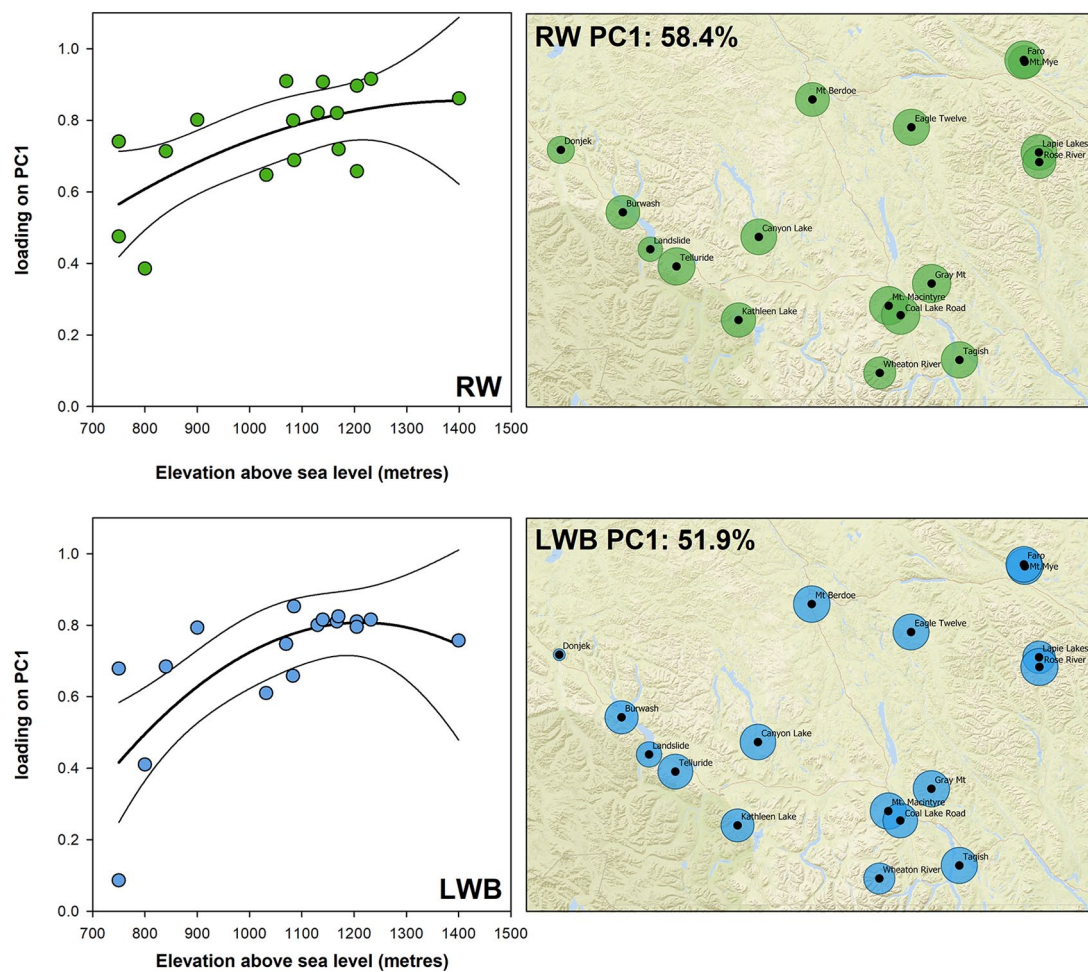


Figure 2. Principal component analysis (PCA) (1856–1997) loadings of each site chronology on the first principal component using the ADSne-sf chronology versions. Left: loadings plotted against site elevation. Non-linear relationship is shown using a second-order polynomial function (with 2-sigma error); right: loading values plotted spatially. The circle size is proportional to the loading value. Similar results are obtained using the different detrending options (Table 2 – results not shown).

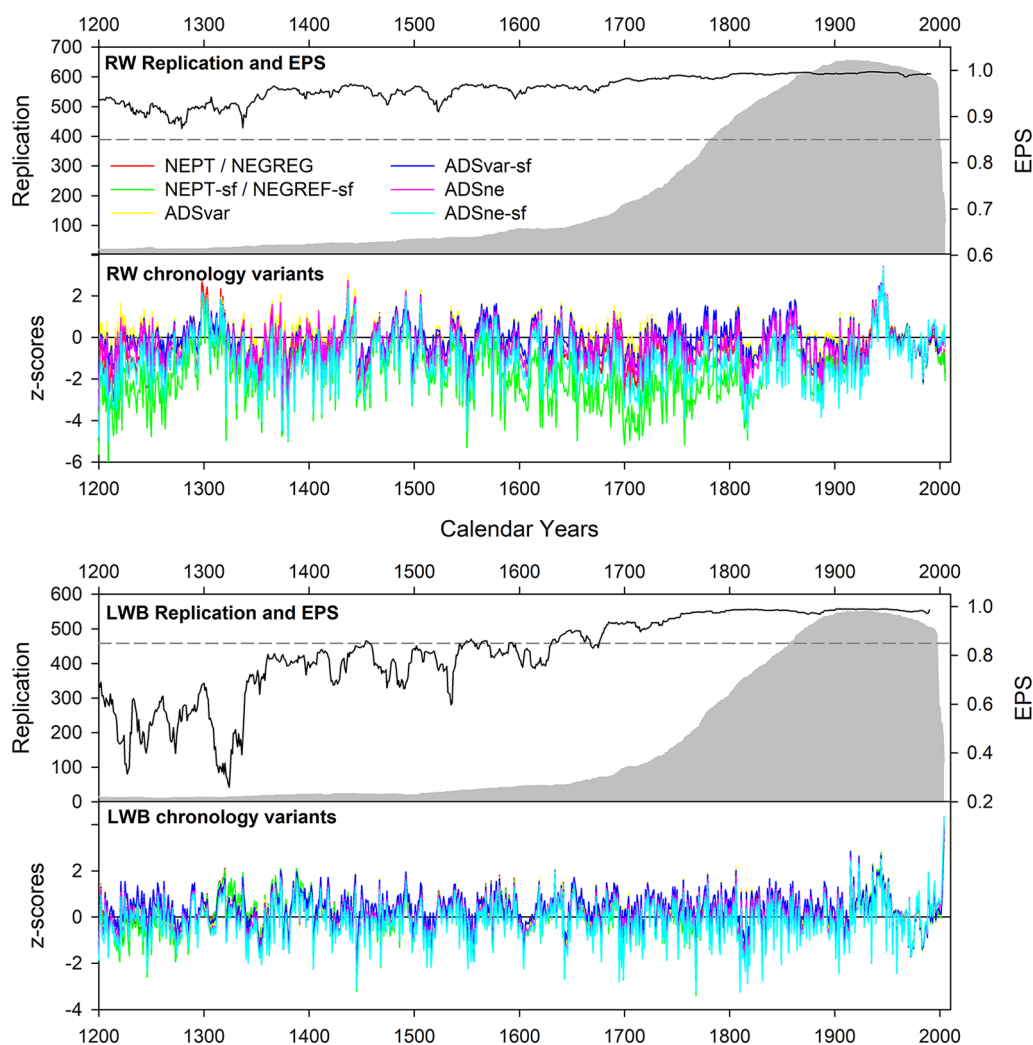


Figure 3. Regional composite chronologies: replication, Expressed Population Signal strength (ADSne-sf version) and chronology variants. To accentuate potential differences in the past, the chronologies are transformed to z-scores relative to the 1944–1997 period.

Climate response

In this region, the T_{max} correlations with RW are generally stronger than T_{mean} (Youngblut and Luckman, 2008). This is also the case for LWB (see below). Correlations between the regional chronology variants and monthly and seasonal T_{max} (Figure 4) show that RW has the greatest coherence with the June temperatures ($r = 0.44$ to 0.53), although similar correlation coefficients are also observed with the May–June (MJ) and June–July (JJ) seasons. Since Youngblut and Luckman (2008) reconstructed JJ T_{max} , we will focus on this season for all further RW-based analyses. The LWB composite chronologies have significant correlations with the May, June, July and August temperatures, although all are weaker than the RW correlation with June. Substantially stronger correlations are found between the LWB chronologies and May–August temperature ($r = 0.65$ – 0.71). It must be emphasised that both the RW and LWB correlations, with their respective optimal month or season, are consistently stronger with their ADSne-sf variants than their traditional (NEPT for RW and NEGREG for LWB) detrending variants.

Focusing on the ADSne-sf variants of the individual chronologies, the median correlation of the RW chronologies with JJ T_{max} is 0.40 ($r = -0.02$ to 0.61). When mapping the strength of each correlation at each site (Figure 5), the spatial pattern is similar to the PC loadings (Figure 2). This suggests that summer temperature is the main factor driving the common signal expressed across the network. Specifically, it is again Donjek and Landslide that have the weakest coherence with temperature, although

Kathleen Lake also demonstrates non-significant correlations. The Kathleen Lake site is another ecologically distinct site, located at the toe of an active rock glacier, so the signal may well be weakened by geomorphic activity. In a similar way, as noted by the change in PC loadings (Figure 2), the RW climate response with temperatures weakens at lower elevations ($< \sim 900$ m a.s.l.; Figure 5). This indicates that those chronologies that load strongly on PC1 also possess the strongest temperature signal. The LWB chronologies have a similar spatial and elevational pattern to RW, although more LWB correlations are significant, suggesting LWB might be less susceptible to site ecological conditions (see also Rydval et al., 2018). The median LWB correlation with MJJA T_{max} is 0.52 ($r = -0.08$ to 0.72) with Donjek again showing the weakest correlation (Figure 5).

To explore the implications of a potential elevation-related response change for dendroclimatic reconstruction, the regional data were divided into two elevational composite records (low and high) around 900 m – the elevation where the RW response to JJ T_{max} temperatures suggests the transition occurs (Figure 5). The four sites that make up the low elevation composite are Burwash, Landslide, Kathleen Lake and Donjek (see Table 1). The elevational composite chronologies were detrended using ADSne-sf to maximise the climate response of both TR variables (Figure 4). The relationship between the low- and high-elevation RW and LWB chronologies is variable through time (Figure 6), but overall the sliding 31-year correlations are positive and generally significant. The RW data express short periods of weak correlation at the

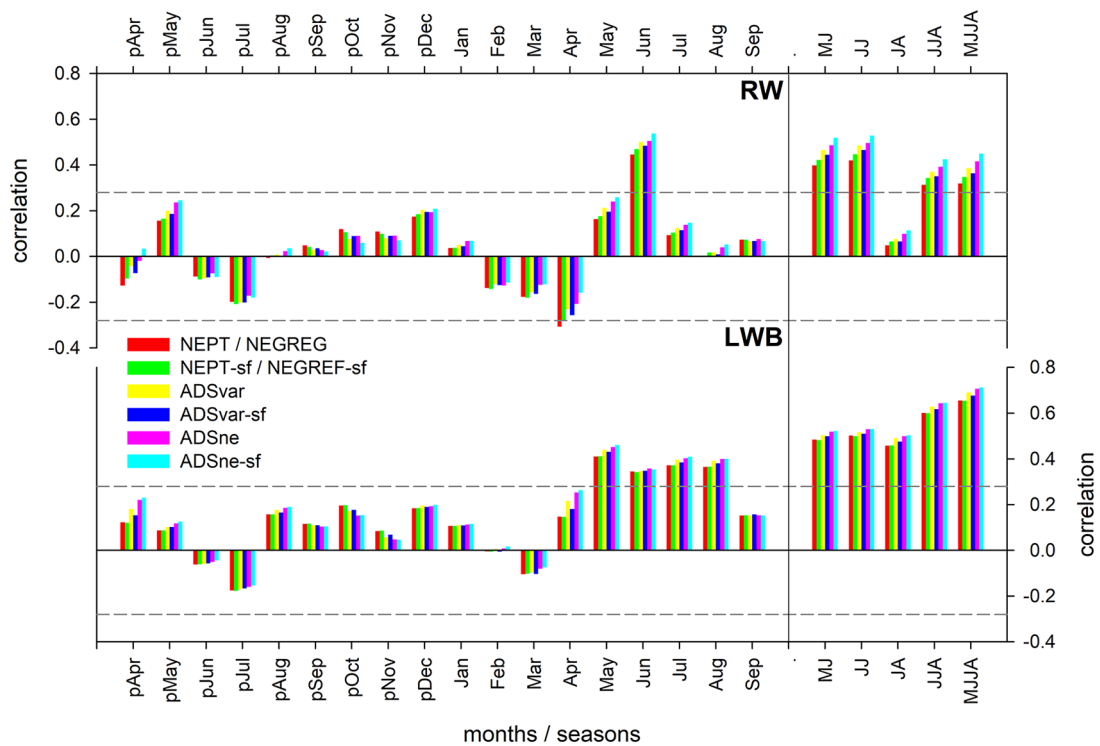


Figure 4. Correlation response function analysis (1944–1997) results for full regional composite chronologies against monthly and seasonal maximum temperatures. Dashed horizontal lines denote the 95% confidence limit.

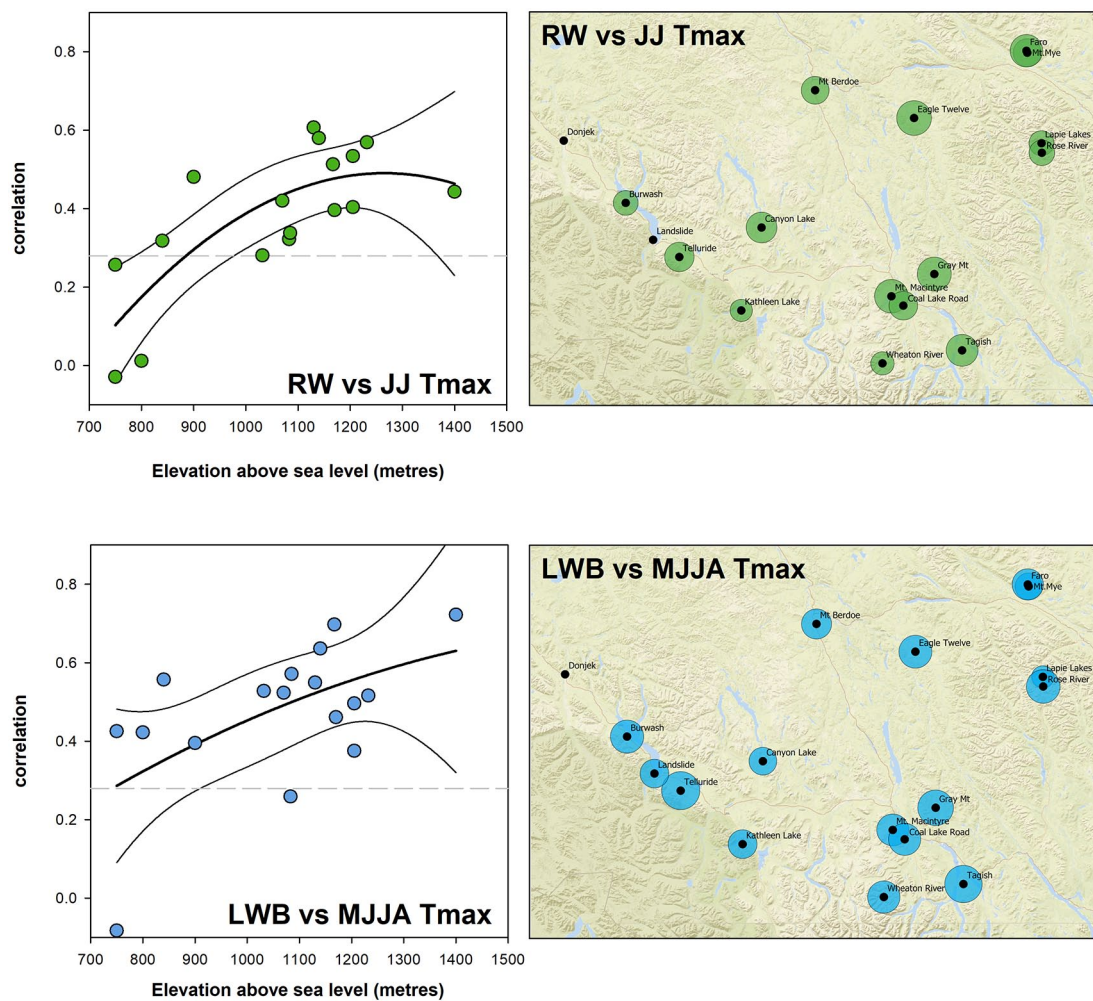


Figure 5. Individual site chronology (ADSne-sf) correlations against June–July (RW) and MJJA (LWB) maximum temperatures. Left: correlations plotted against site elevation. Dashed horizontal lines denote the 95% confidence limit. Non-linear relationship is shown using a second-order polynomial function (with 2-sigma error); right: correlations plotted spatially. Circle size is proportional to the correlation value.

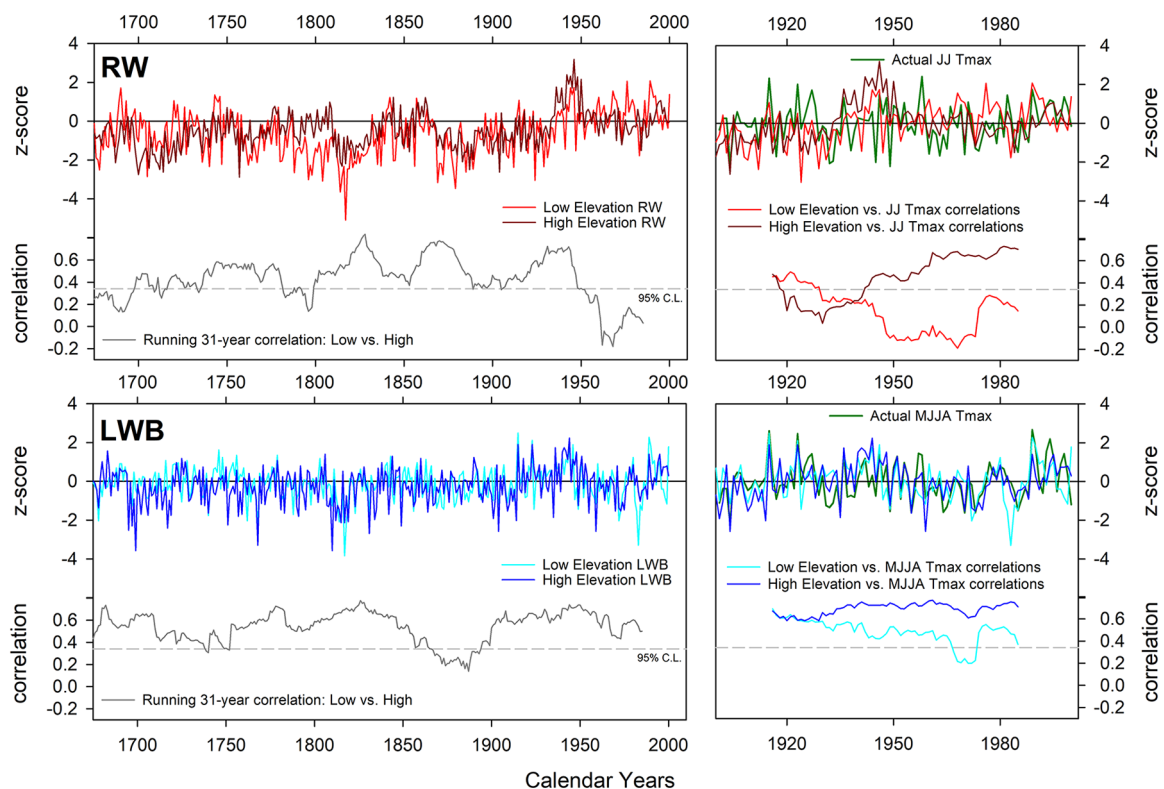


Figure 6. Left: comparison of low- (<900 m a.s.l.) and high-elevation regional composite chronologies (detrended using ADSne-sf) for RW and LWB. The chronology period shown is expressed by a minimum replication of 30 series. The horizontal dashed line denotes the 95% confidence limit for the running 31-year correlations between the records. Right: Low- and high-elevation chronologies compared with the respective optimal temperature seasons (JJ Tmax for RW and MJJA Tmax for LWB) – including running 31-year correlations. Time-series have been transformed to z-scores relative to the 1901–2000 period.

end of the 17th and 18th centuries, but more importantly show a substantial loss in coherence from the mid-20th century. This may be related to the fact that the dominant environmental factor modulating growth at different altitudes has changed in recent decades. A weakening in the agreement between low- and high-elevation LWB chronologies is seen in the latter half of the 19th century, but no de-coupling is found in the 20th century. When compared with temperature, the low-elevation RW composite shows initial significance but then a marked drop in correlation that mirrors the decreased coherence between the low- and high-elevation chronologies. The high-elevation RW record starts with a weak non-significant relationship with JJ Tmax, but then increases until correlations are >0.60 by the end of the 20th century. The high-elevation LWB data shows a stable response with MJJA Tmax with correlations >0.6 throughout the 20th century. The low-elevation LWB expresses a weaker, and slightly weakening, correlation with temperature but still ranging between 0.4 and 0.5. The exception is a short period of non-significance that is likely related to the 1983 low index outlier.

The low-elevation RW and LWB composite's decreasing correlations with temperature through the 20th century (Figure 6) suggests a weakening in temperature limitation on tree-growth at elevations below ~900 m, potentially because of the ca. 1°C warming observed since the 1940s (for both mean and maximum summer temperatures). Overall, the RW data from both elevations do not have a time-stable response to JJ Tmax and do not track decadal trends well. The RW peak growth occurs in the 1940s, especially at high elevations, but it is not associated with the highest temperatures in the instrumental data (Figure 6). Similar observations have been noted for RW chronologies in the northern Yukon and Alaska (Porter and Pisarcic, 2011; Sullivan et al., 2016). The RW data will therefore not be used for producing a dendroclimatic reconstruction for the region, although calibration/validation tests are performed. However, the high-elevation LWB data show

a stable response with temperature and even the low-elevation LWB sites show only a minimal weakening in their climate response. Both the low- and high-elevation LWB records track the trends in MJJA Tmax well (Figure 6) and overall indicate a much stronger and more temporally stable relationship with temperature than RW.

Climatic reconstruction and regional expression

All the site LWB data were composited in order to derive a regional temperature reconstruction. Although the lower elevation LWB sites have a slightly weaker climate signal (Figure 6), the long Landslide chronology (800 m a.s.l.; Table 1) will allow a significant temporal extension to previous work (Youngblut and Luckman, 2008). However, we use an individual series nesting approach (Meko, 1997) to quantify the weakening in climate signal back in time, which reflects both the decreasing replication and the shifting balance to more lower elevation sites.

The chronology/temperature correlations presented so far have focused only on Tmax (Figures 4–6) as this climate variable has been previously shown to be a stronger correlate with RW than Tmean (Youngblut and Luckman, 2008). We not only confirm here that this is also the case for LWB, but that calibration/validation results with Tmax are substantially stronger for LWB than RW (Table 5). Focusing on LWB, calibration (1944–1997) r^2 values range from 0.34 (NEGREG) to 0.45 (ADSne-sf) for Tmean with a higher range of 0.43–0.51 for the same chronology variants against Tmax (Table 5). Validation (combined 1901–1943/1998–2004 period) is also much weaker against Tmean than Tmax, with RE and CE values being mostly negative. For Tmax, all LWB chronology variants express positive RE and CE values, with only the ADSne and ADSne-sf variants passing residual analyses (Table 5). These results highlight that the detrending option and climate target used have a

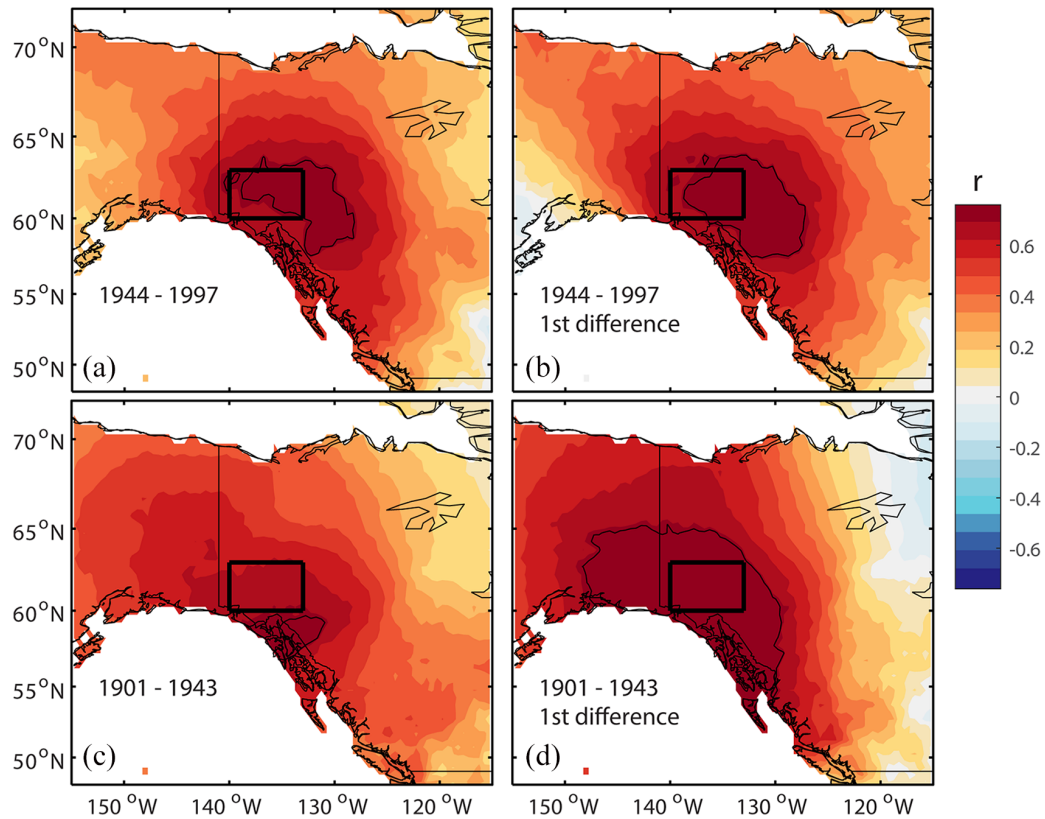
Table 5. Calibration (1944–1997) and validation (1901–1943/1998–2004) results for RW and LWB against Tmean and Tmax. Full period calibration r^2 values calculated over 1901–2004 period.

| RW Tmean | | | | | | | RW Tmax | | | | | | |
|------------|-------|---------|--------|-----------|-------|----------|------------|-------|---------|--------|-----------|-------|----------|
| | NEPT | NEPT-sf | ADSvar | ADSvar-sf | ADSne | ADSne-sf | | NEPT | NEPT-sf | ADSvar | ADSvar-sf | ADSne | ADSne-sf |
| Cal r^2 | 0.13 | 0.15 | 0.20 | 0.17 | 0.21 | 0.26 | Cal r^2 | 0.18 | 0.20 | 0.24 | 0.22 | 0.25 | 0.28 |
| DW | 1.56 | 1.53 | 1.49 | 1.51 | 1.52 | 1.49 | DW | 1.73 | 1.70 | 1.67 | 1.68 | 1.71 | 1.68 |
| Lin r | 0.45 | 0.46 | 0.45 | 0.46 | 0.46 | 0.43 | Lin r | 0.36 | 0.35 | 0.32 | 0.34 | 0.32 | 0.28 |
| Val r^2 | 0.03 | 0.05 | 0.13 | 0.10 | 0.14 | 0.18 | Val r^2 | 0.03 | 0.04 | 0.08 | 0.07 | 0.09 | 0.10 |
| Val RE | 0.05 | 0.12 | 0.14 | 0.14 | 0.19 | 0.25 | Val RE | −0.06 | −0.18 | 0.02 | −0.01 | −0.03 | −0.35 |
| Val CE | −0.09 | 0.00 | 0.02 | 0.02 | 0.08 | 0.14 | Val CE | −0.06 | −0.18 | 0.01 | −0.01 | −0.03 | −0.35 |
| Full r^2 | 0.08 | 0.12 | 0.17 | 0.15 | 0.19 | 0.24 | Full r^2 | 0.09 | 0.09 | 0.15 | 0.13 | 0.15 | 0.14 |

| LWB Tmean | | | | | | | LWB Tmax | | | | | | |
|------------|--------|-----------|--------|-----------|-------|----------|------------|--------|-----------|--------|-----------|-------|----------|
| | NEGREG | NEGREG-sf | ADSvar | ADSvar-sf | ADSne | ADSne-sf | | NEGREG | NEGREG-sf | ADSvar | ADSvar-sf | ADSne | ADSne-sf |
| Cal r^2 | 0.34 | 0.34 | 0.41 | 0.38 | 0.44 | 0.45 | Cal r^2 | 0.43 | 0.43 | 0.48 | 0.46 | 0.50 | 0.51 |
| DW | 1.11 | 1.10 | 1.21 | 1.16 | 1.29 | 1.31 | DW | 1.31 | 1.31 | 1.42 | 1.36 | 1.48 | 1.49 |
| Lin r | 0.52 | 0.52 | 0.46 | 0.50 | 0.41 | 0.40 | Lin r | 0.41 | 0.42 | 0.33 | 0.38 | 0.26 | 0.25 |
| Val r^2 | 0.38 | 0.38 | 0.44 | 0.42 | 0.46 | 0.45 | Val r^2 | 0.48 | 0.48 | 0.50 | 0.50 | 0.46 | 0.45 |
| Val RE | −0.07 | −0.06 | 0.06 | −0.06 | 0.13 | 0.14 | Val RE | 0.33 | 0.33 | 0.40 | 0.34 | 0.37 | 0.35 |
| Val CE | −0.25 | −0.25 | −0.11 | −0.25 | −0.03 | −0.02 | Val CE | 0.33 | 0.33 | 0.40 | 0.34 | 0.37 | 0.35 |
| Full r^2 | 0.26 | 0.26 | 0.33 | 0.28 | 0.37 | 0.38 | Full r^2 | 0.42 | 0.42 | 0.47 | 0.45 | 0.46 | 0.46 |

RW: ring width; Cal r^2 = Calibration r^2 ; DW: Durbin-Watson statistic for residual autocorrelation; Lin r: correlation of linear trend in residuals; RE: reduction of error; CE: coefficient of efficiency; LWB: latewood blue intensity.

Validation metrics highlighted in grey are non-significant.

**Figure 7.** Spatial correlations of ADSne-sf reconstruction with MJJA Tmax for the period 1944–1997 ((a) and (b) are for non-transform and first differenced correlations) and 1901–1943 ((c) and (d) – as for (a) and (b)). Study region denoted by box while black contour denotes region where r^2 is ≥ 0.50 .

substantial influence on the calibration/validation metrics, and that ADSne (with or without SF) appears to be a superior standardisation method for retaining the temperature variations at timescales represented by the instrumental data, especially when associated with the SF approach.

Over the 1944–1997 period the spatial distribution of correlations, produced by both the non-transformed and first differenced versions of the new southern Yukon reconstruction (hereafter denoted as SYBI) and gridded CRU TS temperatures, are very similar (Figure 7a and b). In fact, SYBI explains $>50\%$ of the

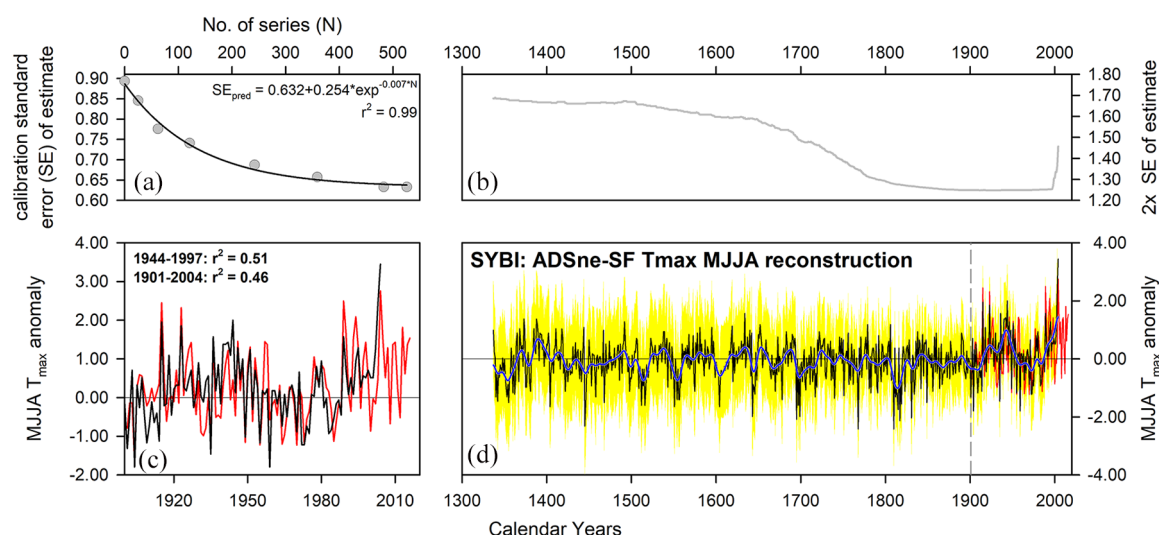


Figure 8. (a) Sub-set nested modelling (Meko, 1997) using the calibration period (1944–1997) to model the change in the standard error (SE) of regression estimate as replication decreases. Start dates (no. of TR series) of the nests were 1944 (526), 1850 (483), 1800 (242), 1750 (121), 1700 (62) and 1650 (25). The non-linear negative exponential function was used to model the relationship between SE and N. (b) Modelled 2× SE using the replication of the LWB data (Figure 3) and the relationship shown in (a). (c) Comparison of actual (red) and reconstructed (black) May–August maximum temperatures. (d) Full southern Yukon (SYBI) reconstruction with 20-year Gaussian smoother.

temperature variance for not only much of the study region, but also down into northern British Columbia. Performing the same analysis from 1901 to 1943 between the gridded CRU temperatures and the non-transformed reconstruction (Figure 7c), the concentration of maximum correlation is shifted to a small region in the south-eastern end of the Gulf of Alaska (centred on the Juneau station – Figure 1). However, after a first difference transform (Figure 7d), the region of strongest spatial correlation increases substantially. These observations suggest that there is some degree of dissimilarity at decadal and longer timescales between SYBI and the pre-1940s instrumental data. Although there could be low frequency biases in the LWB composite chronology, it must be emphasised that the early CRU gridded data over this region are interpolated from instrumental measurements (Figure 1, Table 3) outside the study area that might not fully capture the climate of the study region. It is also possible that there are homogeneity issues (Peterson et al., 1998) in the individual station data. Despite these observations, the ADSne LWB chronologies calibrate and validate well (Table 5).

SYBI tracks 20th and 21st century May–August T_{max} very well (Figure 8) with only a minimal non-significant decrease of calibration r^2 from 0.51 to 0.46 between the calibration (1944–1997) and full (1901–2004) periods (Table 5). The top five warmest reconstructed years (2004, 2003, 1944, 1915 and 1923) are in the 20th/21st centuries (Table 6) and three of the warmest decades (1995–2004, 1939–1948 and 1915–1934) also occurred during this period. The five coldest years are 1768, 1810, 1445, 1817 and 1695, three of which coincide within a year or two following major tropical volcanic eruptions (unknown 1694, unknown 1808 and Tambora 1815 – Sigl et al. 2015). The coldest decade (1810–1819) again reflects large-scale volcanically forced cooling seen in many temperature-sensitive TR records across the NH (Anchukaitis et al., 2017; Briffa et al., 1996; D’Arrigo et al. 2013; Esper et al., 2018; Wilson et al., 2016).

Comparison of SYBI with other regional TR-based summer temperature reconstructions (see Figure 1 for locations) highlights a clear common multi-decadal pattern for a substantial region of NW Northern America (Figure 9). The 20th century is consistently the warmest period in all the records. The coldest decade in SYBI (1810–1819 – Table 6) is also strongly expressed in most series except for Firth River, Alaska, which is located much further north (Figure 1). All records indicate cool conditions around 1700, with

Table 6. Top 5 warmest and coldest years and decades in the SYBI summer maximum temperature reconstruction.

| Warmest | Years | Anomaly | Decades | Anomaly |
|---------|-------|---------|-----------|---------|
| 1 | 2004 | 1.99 | 1995–2004 | 1.15 |
| 2 | 2003 | 1.07 | 1939–1948 | 1.00 |
| 3 | 1944 | 0.75 | 1385–1394 | 0.74 |
| 4 | 1915 | 0.71 | 1915–1924 | 0.52 |
| 5 | 1923 | 0.61 | 1650–1659 | 0.48 |
| Coldest | Years | Anomaly | Decades | Anomaly |
| 1 | 1768 | −3.77 | 1810–1819 | −1.17 |
| 2 | 1810 | −3.70 | 1550–1559 | −0.86 |
| 3 | 1445 | −3.99 | 1508–1517 | −0.79 |
| 4 | 1817 | −3.41 | 1351–1360 | −0.76 |
| 5 | 1695 | −3.59 | 1695–1704 | −0.69 |

1695–1704 being the fifth coolest decade in SYBI, another period of consistent cooling across the NH (Wilson et al., 2016). Running 31-year correlations between SYBI and the other reconstructions show the strongest coherence with the Wrangells MXD record, which is not surprising as LWB and MXD are often strongly correlated (Wilson et al., 2014); the two regions are closely located, and both express more continental-style climatic conditions compared with the Gulf of Alaska. The correlations of SYBI with the other reconstructions are temporally less stable than with the Wrangells, with multi-decadal periods (centred around the 1660s, 1760s, 1880s and the late 20th century) showing non-significant correlations. These periods of weaker coherence likely represent differences in the seasonal climate signal expressed by the different TR variables (RW, MXD and delta BI) as well as dynamical differences between the regions. However, the SYBI comparison with the longer reconstructions from the Gulf of Alaska (RW – Wiles et al., 2014) and Firth River (MXD – Anchukaitis et al., 2013) shows a marked decrease in coherence prior to the early 17th century when replication in SYBI drops below 50 series (with associated increased uncertainty, Figure 8a and 8b) and the data predominantly shift to the lower elevation Landslide site. This early period in the SYBI should therefore be used cautiously.

Finally, the biggest difference between SYBI and the other records is that it does not appear to capture as much centennial and

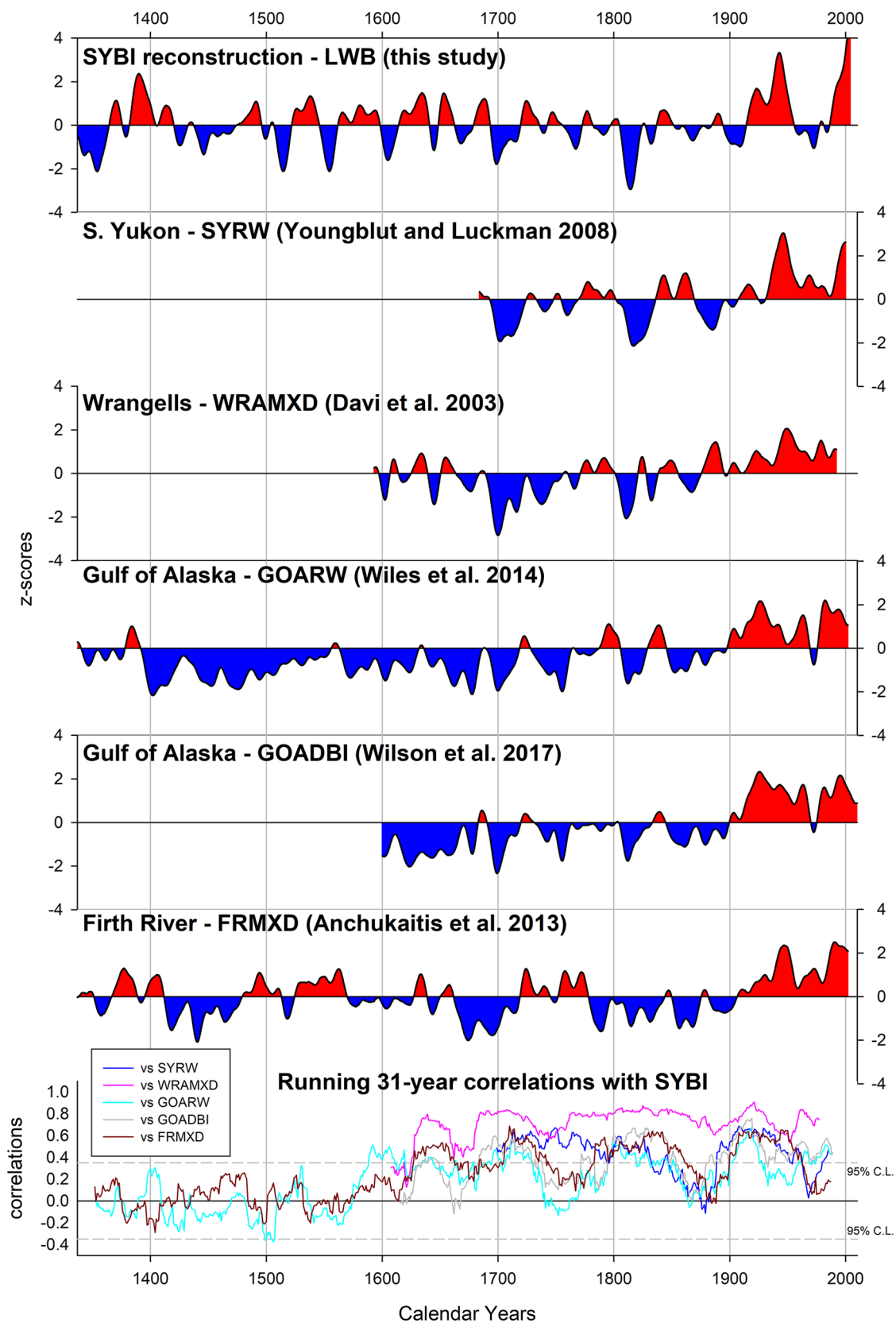


Figure 9. Low-pass filter (20-year Gaussian) comparison between SYBI and other regional summer temperature reconstructions for north-western North America. All series transformed to z-scores relative to the common period. The lower panel shows running 31-year correlations between SYBI and the other regional reconstructions.

longer timescale variability over the past 600 years. Even using ADS within the SF framework will result in a loss of low-frequency information at timescales longer than the mean length of the samples (Cook et al., 1995). Only the Gulf of Alaska (Wiles et al., 2014) and Firth River (Anchukaitis et al., 2013) reconstructions have been processed using methods capable of overcoming the

‘segment length curse’ (Briffa et al., 1996; Briffa and Melvin, 2011; Cook et al., 1995). At this time, no regional curve standardisation (RCS) experiments have been performed as the current living tree regional dataset, with very high replication in the recent period, could contribute a significant ‘modern sample’ bias to the resultant chronology (Anchukaitis et al., 2013; Melvin and Briffa, 2014).

Summary and conclusion

Recent large-scale network analyses using temperature-sensitive TR data have highlighted how little data for North America extend back to the Medieval period (Anchukaitis et al., 2017; Esper et al., 2018; Guillet et al., 2017; Wilson et al., 2016). Dendroclimatic efforts must focus on sampling new regions and extending previous reconstructions back in time. Despite the superiority of MXD as a proxy of past summer temperatures (Anchukaitis et al., 2012; Briffa et al., 2002; Büntgen et al., 2006; Esper et al., 2012; Wilson et al., 2016), only one MXD record for North America goes back before 1000 CE (Luckman and Wilson, 2005). Previous work has shown that MXD can overcome the so-called ‘Divergence Problem’ calibration issues noted in RW data from many spruce sites in western Canada and Alaska (Anchukaitis et al., 2013; Andreu-Hayles et al., 2011; Luckman and Wilson, 2005; Sullivan et al., 2016; Wilson and Luckman, 2003). However, the relative expense and lack of facilities for measuring MXD severely hampers the development of new datasets. LWB has received substantial attention as an economically viable substitute for MXD as they both measure similar wood properties of conifer latewood (Björklund et al., 2015, 2014; Campbell et al., 2007; Fuentes et al., 2018; Kaczka et al., 2018; McCarroll et al., 2002; Rydval et al., 2014, 2017a, 2017b, 2018; Wilson et al., 2014, 2017). This paper demonstrates the utility of white spruce LWB chronologies from the southern Yukon. As white spruce covers substantial parts of northern North America (Figure 1), proving LWB’s suitability for producing a robust dendroclimatic reconstruction of past summer temperatures from this species could lead to a substantial enlargement and improvement in the North American temperature-sensitive TR network across the Boreal Taiga.

Despite having a weaker common signal strength than RW, LWB still contains the stronger, and most temporally stable relationship with summer T_{max}. A much weaker and variable temperature response in RW was noted for sites below 900 m a.s.l., although this observation is likely exacerbated by site-specific ecological issues. Nevertheless, the lower elevation LWB data still exhibited enough significant temperature sensitivity to be used for climate reconstruction. For the final reconstruction, the LWB data from all 17 sites were composited into one regional record. This record begins in 1337 CE when replication is ≥ 15 series and EPS is greater than 0.7, with values attaining 0.85 in the mid-17th century. A variety of different detrending options were utilised and the ADS methods (allowing the retention of positive trends), applied within the SF framework, performed markedly better than other methods, resulting in calibration r^2 values over 0.50 (Table 5) and good independent validation based on RE, CE and residual analysis. RW calibration r^2 values never exceeded 0.30, while LWB detrending using linear functions returned weaker calibration results with noted linear trends and significant autocorrelation in the model residuals. The final MJJA T_{max} reconstruction (SYBI) shows excellent spatial coherence over much of the southern Yukon and northern British Columbia. When SYBI is compared with independent TR-based temperature reconstructions from north-western North America, all the records suggest that the 20th century is the warmest 100-year period in the past 600 years.

Overall, LWB is proven to be a robust proxy for reconstructing past summer temperatures from white spruce samples. Most importantly, our findings show that LWB, as with MXD, is not prone to the time-varying response problems noted for RW in North American white spruce. Similar observations were recently made for LWB using Norway spruce (*Picea abies* (L) Karst) in the northern Carpathian Mountains of Europe (Buras et al., 2018). Future work in the southern Yukon will now focus on updating the living network to the present, but most importantly, to sample sub-fossil remnant material extracted from lake sediments to increase replication prior to the 1650s, where current reconstruction uncertainty increases substantially because of low sample replication.

The large area covered by the current living network will allow considerable opportunity for finding appropriate lakes with preserved sub-fossil material at elevations above 900 m a.s.l. where the climate signal is stronger (Figure 6).

Some challenges remain, particularly the darker colouration of preserved sub-fossil samples from lakes in relation to their living wood counterparts. Several methods have been proposed to overcome such colour change biases (Björklund et al., 2014, 2015; Rydval et al., 2017a, 2017b; Wilson et al., 2017), but more experimentation is needed. The increasing number of papers comparing LWB with MXD clearly show the potential of this parameter for reconstructing past summer temperatures (Björklund et al., 2015, 2014; Fuentes et al., 2018; Kaczka et al., 2018; McCarroll et al., 2002; Rydval et al., 2014; Wilson et al., 2014). The blue revolution is upon us, but further methodological development is needed. Generating LWB is inexpensive, making this methodology available to all laboratories with minimal investment. There is no reason why the many spatial gaps across the NH, identified by Anchukaitis et al. (2017), cannot be filled in the coming years.

Funding

The author(s) disclosed receipt of the following financial support for the research, authorship, and/or publication of this article: This work was funded by the US National Science Foundation (NSF) Grants AGS 1159430, AGS 1502186, AGS 1502150, PLR 15-04134, PIRE 1743738, AGS-15-167 and PLR16-03473. The Signal-Free software used for the detrending in this paper is available at <https://www.ldeo.columbia.edu/res/fac/trl/public/ftp/index.php?dir=Public/Software/>. Lamont-Doherty Earth Observatory contribution no. 8328 is also acknowledged.

ORCID iD

R Wilson  <https://orcid.org/0000-0003-4486-8904>

References

- Anchukaitis KJ, Breitenmoser P, Briffa KR et al. (2012) Tree rings and volcanic cooling. *Nature Geoscience* 5(12): 836.
- Anchukaitis KJ, D’Arrigo RD, Andreu-Hayles L et al. (2013) Tree-ring-reconstructed summer temperatures from north-western North America during the last nine centuries. *Journal of Climate* 26(10): 3001–3012.
- Anchukaitis KJ, Wilson K, Briffa U et al. (2017) Last millennium Northern Hemisphere summer temperatures from tree rings: Part II: Spatially resolved reconstructions. *Quaternary Science Reviews* 163: 1–22.
- Andreu-Hayles L, D’Arrigo R, Anchukaitis KJ et al. (2011) Varying boreal forest response to Arctic environmental change at the Firth River, Alaska. *Environmental Research Letters* 6(4): 045503.
- Björklund J, Gunnarson BE, Seftigen K et al. (2015) Using adjusted blue intensity data to attain high-quality summer temperature information: A case study from Central Scandinavia. *The Holocene* 25(3): 547–556.
- Björklund JA, Gunnarson BE, Seftigen K et al. (2014) Blue intensity and density from northern Fennoscandian tree rings, exploring the potential to improve summer temperature reconstructions with earlywood information. *Climate of the past* 10(2): 877–885.
- Briffa KR and Melvin TM (2011) A closer look at regional curve standardization of tree-ring records: Justification of the need, a warning of some pitfalls, and suggested improvements in its application. In: Hughes MK, Swetnam TW and Diaz HF (eds) *Dendroclimatology*. Dordrecht: Springer, pp. 113–145.
- Briffa KR, Jones PD, Schweingruber FH et al. (1996) Tree-ring variables as proxy-climate indicators: Problems with low-frequency signals. In: Jouzel J, Bradley RS and Jones P (eds)

- Climatic Variations and Forcing Mechanisms of the Last 2000 Years*. Berlin: Springer, pp. 9–41.
- Briffa KR, Osborn TJ, Schweingruber FH et al. (2002) Tree-ring width and density data around the Northern Hemisphere: Part 1, local and regional climate signals. *The Holocene* 12(6): 737–757.
- Buckley BM, Hansen KG, Griffin KL et al. (2018) Blue intensity from a tropical conifer's annual rings for climate reconstruction: An ecophysiological perspective. *Dendrochronologia* 50: 10–22.
- Büntgen U, Frank DC, Nievergelt D et al. (2006) Summer temperature variations in the European Alps, AD 755–2004. *Journal of Climate* 19(21): 5606–5623.
- Buras A, Spyt B, Janecka K et al. (2018) Divergent growth of Norway spruce on Babia Góra Mountain in the western Carpathians. *Dendrochronologia* 50: 33–43.
- Campbell R, McCarroll D, Loader NJ et al. (2007) Blue intensity in *Pinus sylvestris* tree-rings: Developing a new palaeoclimate proxy. *The Holocene* 17(6): 821–828.
- Cook ER, Briffa K, Shiyatov S et al. (1990) Tree-ring standardisation and growth-trend estimation. In: Cook ER and Kairiukstis LA (eds) *Methods of Dendrochronology: Applications in the Environmental Sciences*. Dordrecht: Kluwer Academic Publishers, pp. 104–123.
- Cook ER, Briffa KR and Jones PD (1994) Spatial regression methods in dendroclimatology: A review and comparison of two techniques. *International Journal of Climatology* 14(4): 379–402.
- Cook ER, Briffa KR, Meko DM et al. (1995) The 'segment length curse' in long tree-ring chronology development for palaeoclimatic studies. *The Holocene* 5(2): 229–237.
- D'Arrigo R, Wilson R and Anchukaitis KJ (2013) Volcanic cooling signal in tree ring temperature records for the past millennium. *Journal of Geophysical Research Atmospheres* 118(16): 9000–9010.
- D'Arrigo R, Wilson R, Liepert B et al. (2008) On the 'divergence problem' in northern forests: A review of the tree-ring evidence and possible causes. *Global and Planetary Change* 60(3–4): 289–305.
- Davi NK, Jacoby GC and Wiles GC (2003) Boreal temperature variability inferred from maximum latewood density and tree-ring width data, Wrangell Mountain region, Alaska. *Quaternary Research* 60(3): 252–262.
- Esper J, Frank D, Büntgen U et al. (2007) Long-term drought severity variations in Morocco. *Geophysical Research Letters* 34(17): L17702.
- Esper J, Frank DC, Timonen M et al. (2012) Orbital forcing of tree-ring data. *Nature Climate Change* 2(12): 862.
- Esper J, George SS, Anchukaitis K et al. (2018) Large-scale, millennial-length temperature reconstructions from tree-rings. *Dendrochronologia* 50: 81–90.
- Fritts HC (1976) *Tree Rings and Climate*. San Diego, CA: Academic, p. 567.
- Fritts HC, Mosimann JE and Bortorff CP (1969) A revised computer program for standardizing tree-ring series. *Tree-Ring Bulletin* 29: 15–20.
- Fuentes M, Salo R, Björklund J et al. (2018) A 970-year-long summer temperature reconstruction from Rogen, west-central Sweden, based on blue intensity from tree rings. *The Holocene* 28(2): 254–266.
- Gennaretti F, Arseneault D, Nicault A et al. (2014) Volcano-induced regime shifts in millennial tree-ring chronologies from northeastern North America. *Proc Natl Acad Sci USA* 111: 10077–10082.
- Guillet S, Corona C, Stoffel M et al. (2017) Climate response to the Samalas volcanic eruption in 1257 revealed by proxy records. *Nature Geoscience* 10(2): 123.
- Harris I, Philip J, Osborn T et al. (2014) Updated high-resolution grids of monthly climatic observations—the CRU TS3.10 Dataset. *International Journal of Climatology* 34(3): 623–642.
- Holmes RL, Adams RK and Fritts HC (1986) Tree-ring chronologies of western North America: California, eastern Oregon and northern Great Basin with procedures used in the chronology development work including users manuals for computer programs COFECHA and ARSTAN. Available at: <https://www.worldcat.org/title/tree-ring-chronologies-of-western-north-america-california-eastern-oregon-and-northern-great-basin-with-procedures-used-in-the-chronology-development-work-including-users-manuals-for-computer-programs-cofecha-and-arstan/oclc>
- Jacoby GC and D'Arrigo RD (1995) Tree ring width and density evidence of climatic and potential forest change in Alaska. *Global Biogeochemical Cycles* 9(2): 227–234.
- Kaczka RJ, Spyt B, Janecka K et al. (2018) Different maximum latewood density and blue intensity measurements techniques reveal similar results. *Dendrochronologia* 49: 94–101.
- Luckman BH and Wilson RJS (2005) Summer temperatures in the Canadian Rockies during the last millennium: A revised record. *Climate Dynamics* 24(2–3): 131–144.
- McCarroll D, Pettigrew E, Luckman A et al. (2002) Blue reflectance provides a surrogate for latewood density of high-latitude pine tree rings. *Arctic, Antarctic, and Alpine Research* 34(4): 450–453.
- Meko D (1997) Dendroclimatic reconstruction with time varying predictor subsets of tree indices. *Journal of Climate* 10(4): 687–696.
- Melvin TM and Briffa KR (2008) A 'signal-free' approach to dendroclimatic standardisation. *Dendrochronologia* 26(2): 71–86.
- Melvin TM and Briffa KR (2014) CRUST: Software for the implementation of regional chronology standardisation: Part 1. Signal-free RCS. *Dendrochronologia* 32(1): 7–20.
- Melvin TM, Briffa KR, Nicolussi K et al. (2007) Time-varying-response smoothing. *Dendrochronologia* 25(1): 65–69.
- Peterson TC, Easterling DR, Karl TR et al. (1998) Homogeneity adjustments of in situ atmospheric climate data: A review. *International Journal of Climatology: A Journal of the Royal Meteorological Society* 18(13): 1493–1517.
- Porter TJ and Pisaric MF (2011) Temperature-growth divergence in white spruce forests of Old Crow Flats, Yukon Territory, and adjacent regions of northwestern North America. *Global Change Biology* 17(11): 3418–3430.
- Rydval M, Druckenbrod DL, Svoboda M et al. (2018) Influence of sampling and disturbance history on climatic sensitivity of temperature-limited conifers. *The Holocene* 28(10): 1574–1587.
- Rydval M, Gunnarson BE, Loader NJ et al. (2017a) Spatial reconstruction of Scottish summer temperatures from tree rings. *International Journal of Climatology* 37(3): 1540–1556.
- Rydval M, Larsson LÅ, McGlynn L et al. (2014) Blue intensity for dendroclimatology: Should we have the blues? Experiments from Scotland. *Dendrochronologia* 32(3): 191–204.
- Rydval M, Loader NJ, Gunnarson BE et al. (2017b) Reconstructing 800 years of summer temperatures in Scotland from tree rings. *Climate Dynamics* 49(9–10): 2951–2974.
- Schneider L, Smerdon JE, Büntgen U et al. (2015) Revising mid-latitude summer temperatures back to AD 600 based on a wood density network. *Geophysical Research Letters* 42(11): 4556–4562.
- Schweingruber FH and Briffa KR (1996) Tree-ring density networks for climate reconstruction. In: Jouzel J, Bradley RS and Jones P (eds) *Climatic Variations and Forcing Mechanisms of the Last 2000 Years*. Berlin: Springer, pp. 43–66.
- Sigl M, Winstrup M, McConnell JR et al. (2015) Timing and climate forcing of volcanic eruptions for the past 2,500 years. *Nature* 523(7562): 543.
- Stoffel M, Khodri M, Corona C et al. (2015) Estimates of volcanic-induced cooling in the Northern Hemisphere over the past 1,500 years. *Nature Geoscience* 8(10): 784.

- Sullivan PF, Pattison RR, Brownlee AH et al. (2016) Effect of tree-ring detrending method on apparent growth trends of black and white spruce in interior Alaska. *Environmental Research Letters* 11(11): 114007.
- Wigley TM, Briffa KR and Jones PD (1984) On the average value of correlated time series, with applications in dendroclimatology and hydrometeorology. *Journal of Climate and Applied Meteorology* 23(2): 201–213.
- Wiles GC, D'Arrigo RD, Barclay D et al. (2014) Surface air temperature variability reconstructed with tree rings for the Gulf of Alaska over the past 1200 years. *The Holocene* 24(2): 198–208.
- Wilson R and Elling W (2004) Temporal instability in tree-growth/climate response in the Lower Bavarian Forest region: Implications for dendroclimatic reconstruction. *Trees* 18(1): 19–28.
- Wilson R, Anchukaitis K, Briffa K et al. (2016) Last millennium Northern Hemisphere summer temperatures from tree rings: Part I: The long term context. *Quaternary Science Reviews* 134: 1–18.
- Wilson R, D'Arrigo R, Andreu-Hayles L et al. (2017) Experiments based on blue intensity for reconstructing North Pacific temperatures along the Gulf of Alaska. *Climate of the past* 13(8): 1007–1022.
- Wilson R, Rao R, Rydval M et al. (2014) Blue Intensity for dendroclimatology: The BC blues: A case study from British Columbia, Canada. *The Holocene* 24(11): 1428–1438.
- Wilson RJ and Luckman BH (2003) Dendroclimatic reconstruction of maximum summer temperatures from upper treeline sites in Interior British Columbia, Canada. *The Holocene* 13(6): 851–861.
- Youngblut D and Luckman B (2008) Maximum June–July temperatures in the southwest Yukon over the last 300 years reconstructed from tree rings. *Dendrochronologia* 25(3): 153–166.